JACS
JOURNAL OF THE AMERICAN CHEMICAL SOCIETY
Article
pubs.acs.org/JACS

Giant Molecular Shape Amphiphiles Based on Polystyrene–Hydrophilic [60]Fullerene Conjugates: Click Synthesis, Solution Self-Assembly, and Phase Behavior

Xinfei Yu,[‡] Wen-Bin Zhang,[‡] Kan Yue,[‡] Xiaopeng Li,[‡] Hao Liu,[‡] Yu Xin,[‡] Chien-Lung Wang,[‡] Chrys Wesdemiotis,[‡,‡] and Stephen Z. D. Cheng*[,‡]

[‡]Department of Polymer Science, College of Polymer Science and Polymer Engineering, The University of Akron, Akron, Ohio 44325-3909, United States

[‡]Department of Chemistry, The University of Akron, Akron, Ohio 44325-3601, United States

Supporting Information

ABSTRACT: This paper reports a comprehensive study on the synthesis and self-assembly of two model series of molecular shape amphiphiles, namely, hydrophilic [60]fullerene (AC_{60}) tethered with one or two polystyrene (PS) chain(s) at one junction point (PS_n–AC_{60} and $2PS_n$–AC_{60}). The synthesis highlighted the regiospecific multiaddition reaction for C_{60} surface functionalization and the Huisgen 1,3-dipolar cycloaddition between alkyne functionalized C_{60} and azide functionalized polymer to give rise to shape amphiphiles with precisely defined surface chemistry and molecular topology. When 1,4-dioxane/DMF mixture was used as the common solvent and water as the selective solvent, these shape amphiphiles exhibited versatile self-assembled micellar morphologies which can be tuned by changing various parameters, such as molecular topology, polymer tail length, and initial molecular concentration, as revealed by transmission electron microscopy and light scattering experiments. In the low molecular concentration range of equal or less than 0.25 (wt) %, micellar morphology of the series of PS_n–AC_{60} studied was always spheres, while the series of $2PS_n$–AC_{60} formed vesicles. Particularly, PS_{44}–AC_{60} and $2PS_{23}$–AC_{60} are synthesized as a topological isomer pair of these shape amphiphiles. PS_{44}–AC_{60} formed spherical micelles while $2PS_{23}$–AC_{60} generated bilayer vesicles under identical conditions. The difference in the self-assembly of PS_n–AC_{60} and $2PS_n$–AC_{60} was understood by the molecular shape aspect ratio. The stretching ratio of PS tails decreased with increasing PS tail length in the spherical micelles of PS_n–AC_{60}, indicating a micellar behavior that changes from small molecular surfactant-like to amphiphilic block copolymer-like. For the series of PS_n–AC_{60} in the high molecular concentration range [>0.25 (wt) %], their micellar morphological formation of spheres, cylinders, and vesicles was critically dependent upon both the initial molecular concentration and the PS tail length. On the other hand, the series of $2PS_n$–AC_{60} remained in the state of bilayer vesicles in the same concentration range. Combining both of the experimental results obtained in the low and high molecular concentrations, a systematic morphological phase diagram was constructed for the series of PS_n–AC_{60} with different PS tail lengths. The versatile and concentration-sensitive phase behaviors of these molecular shape amphiphiles are unique and have not been systematically explored in the traditional surfactants and block copolymers systems.

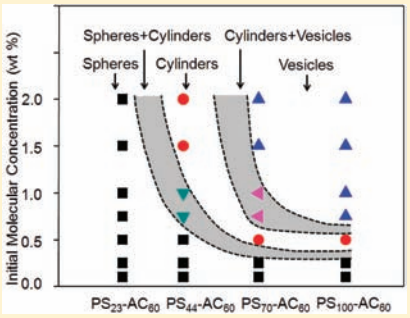

INTRODUCTION

Inspired by Nature, self-assembly is now well-established as the central theme in developing new materials.[1−5] Noncovalent interaction between building blocks is a key parameter for self-assembling process, which was well-demonstrated in the last several decades.[6−11] It was not until recently that the anisotropy and rigidity in shape are also recognized as important parameters in the fine-tuning of self-assembled structures.[12−15] Benefited from the booming nanotechnology, a large variety of nanobuilding blocks with various shapes, different symmetry, distinct topology, and diverse surface chemistry are now available. "Shape amphiphiles" thus refer to entities constructed from these chemically distinct and geometrically anisotropic building blocks.[13,16,17] Computer simulation has predicted various and intriguing hierarchical structures and phase behaviors on these shape amphiphiles.[18−20] The effects of molecular concentration, solvent composition, and so forth on their self-assembly behaviors have also been predicted.[21] However, experimental investigations are relatively preliminary and scarce in literature. To the best of our knowledge, there is yet no systematic report on the phase behavior and various self-assembled morphologies for such shape amphiphiles. It is thus our goal to design and synthesize model shape amphiphiles with precisely controlled molecular topology for a systematic study of their self-assembly and morphological transitions.

Polymer-tethered nanoparticles are a class of prototype "shape amphiphiles". Typical examples include polymer-

Received: January 3, 2012
Published: April 26, 2012

   dx.doi.org/10.1021/ja3000529 | J. Am. Chem. Soc. 2012, 134, 7780−7787

tethered gold particles,[22−24] quantum dots,[25,26] globular protein,[27−30] and molecular nanoparticles (MNPs) such as [60]fullerene (C_{60})[31−34] and polyhedral oligomeric silsesquioxane (POSS),[35−38] among which MNPs are advantageous in providing a precisely defined and readily tunable nanosized structural scaffold. C_{60} has a spherical shape with truncated icosahedral (I_h) symmetry which is an ideal building block for self-assembly system. Well-established fullerene chemistry provides elegant means to functionalize C_{60} in a regiospecific way.[39] Amphiphilic or lipophilic fullerenes have been designed and synthesized based on hydrophobic characteristic of fullerene, which have shown shape-persisted micelles or bilayered vesicles in solution.[40−43] The self-assembled morphologies of these amphiphilic fullerenes are stable but hard to be tuned by changing the physical parameters. On the other hand, although the synthesis of hydrophilic polymer-tethered fullerene has also been reported,[44] there have been limited reports on the self-assembly behaviors of these molecular shape amphiphiles due probably to the unbalanced interaction which leads to irregular aggregates. Recently, our group has constructed "giant surfactants" based POSS with various surface functionalities.[45,46] Self-assembly of one of such giant surfactants, carboxylic-acid-functionalized POSS end-capped polystyrene (PS) (APOSS-PS), leads to various micelles (spheres, cylinders, and vesicles) where the PS tails have been found to be highly stretched, similar to those observed in small-molecule surfactant assemblies.[45] The unique features of the system include the lack of corona in these micelles (when MNPs are present on the surface), the fixed shape and volume of the MNP heads, tailor-made topologies, and the relatively slow self-assembling kinetics (as compared to small-molecule surfactants), which possibly leads to versatile metastable states in phase behaviors.[47] In addition to the factors such as molecular architecture, concentration, solvent properties, pH, ionic strength, and others which are known to affect micellar morphologies,[48−51] it remains an intriguing question how these specific features would impact the self-assembly of the shape amphiphiles.

In this article, we report the design, synthesis, and self-assembly of two series of molecular shape amphiphiles, namely, hydrophilic C_{60} (AC_{60}) tethered with one or two PS chains at one junction point (Scheme 1), PS_n−AC_{60} and $2PS_n$−AC_{60},

Scheme 1. Cartoon Illustration of the Two Molecular Shape Amphiphiles

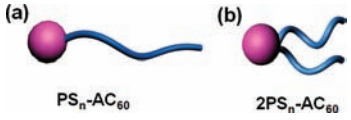

respectively. The philosophy of the current molecular design is to use hydrophilic fullerene as the polar head, which is different from those precedent amphiphilic fullerenes reported in the literature that used fullerene cage as the persist hydrophobic block.[40−43] In this way, the fullerene is only used as a nano structural scaffold with fixed volume and shape. While the electronic property of C_{60} might be lost in these shape amphiphiles, the surface functionalization with multiple interactions aids in the self-assembly of the resulting amphiphiles, giving rise to diverse morphologies. Moreover, it is possible to recover the valuable electronic properties of C_{60} by controlled potential electrolysis to remove all the malonates after self-assembled morphologies have been formed and fixed.[52] Conjugation of functionalized C_{60} with PS chains was achieved via the Huisgen 1,3-dipolar cycloaddition "click" reaction. The difference in molecular topology (one tail vs two tails) turns out to be critical in determining their self-assembled morphologies under identical conditions besides other important factors such as PS tail length, initial molecular concentration, and solvent properties. The study here provides the first systematic experimental illustration of the self-assembly of molecular shape amphiphiles in solutions and the effects of molecular topology, initial molecular concentration, and polymer tail length on these assembled morphologies.

RESULTS AND DISCUSSION

Molecular Design and Synthetic Route. Three parameters are very important in the molecular design of shape amphiphiles: (1) shape; (2) interaction; and (3) topology. In our system, the C_{60} head is regiospecifically functionalized with 10 carboxylic acid groups, which impart hydrophilicity on the surface of C_{60}. The rigid shape and fixed volume, together with the installation of 10 carboxylic acid groups that provides multivalent interactions, make AC_{60} an ideal building block to construct shape amphiphiles. Molecular topology was controlled by the use of precisely defined fullerene derivative precursors and "click" chemistry. Tethering one or two PS chains to a single point on AC_{60} brings in the topological variance. The synthetic route was outlined in Scheme 2. First, Bingel-Hirsch cyclopropanation reaction is well-established for the preparation of various hexakisadducts of C_{60}.[53,54] [5:1]-Hexakisadducts of C_{60} were synthesized by sequential cyclopropanation to give "clickable" C_{60} derivatives **5a**−**b**, carrying one or two terminal alkyne groups and 10 protected carboxylic acid groups. These reactions give moderate to decent yields for fullerene multifunctionalization (∼ 46% for C_{60} functionalization and ∼80% for desilylation, see Supporting Information for details), and the structures of alkyne-functionalized fullerenes (fullerynes) **4a**−**b**, **5a**−**b** were confirmed by ^{1}H NMR and ^{13}C NMR spectra as well as MALDI-TOF mass spectra (Figures S1−S4 in Supporting Information). Particularly, the T_h-symmetry of the carbon cage was confirmed by the ^{13}C NMR spectra in Supporting Information Figure S1, where the sp^3 carbon atoms show up at δ = 69.0 ppm and the only two different types of sp^2 carbons have chemical shifts around δ = 145.9 and 140.8 ppm, respectively.[55]

Second, the Huisgen 1,3-dipolar cycloaddition of azide−alkyne has been well-known as a model "click" reaction that is highly efficient, modular, and robust.[56] It has been widely applied to overcome difficulties in doing chemistry with fullerene or to ensure well-defined structures with high fullerene functionality.[32,57,58] Here, azide functionalized PS (PS_n−N_3, where n is the number average degree of polymerization) was prepared via atom transfer radical polymerization (ATRP) and subsequent nucleophilic substitution with sodium azide in DMF. "Click" reactions between AC_{60} and PS_n−N_3 proceed efficiently to give the desired shape amphiphiles with diverse topology. **6a** (PS_n−tC_{60}) and **6b** ($2PS_n$−tC_{60}) were obtained with a yield of 80% and 70%, respectively. Deprotection of the *tert*-butyl esters on **6a** and **6b** with trifluoroacetic acid in dichloromethane reveals the amphiphilic feature of PS_n−AC_{60} and $2PS_n$−AC_{60} in high yields (∼ 95%).

The success of the "click" reaction and deprotection was confirmed by size exclusion chromatograph (SEC), FT-IR, ^{1}H NMR, and ^{13}C NMR spectra (see Figures S5−S8 in Supporting

dx.doi.org/10.1021/ja3000529 | J. Am. Chem. Soc. 2012, 134, 7780−7787

Scheme 2. Syntheses of PS_n–AC_{60} and $2PS_n$–AC_{60}[a]

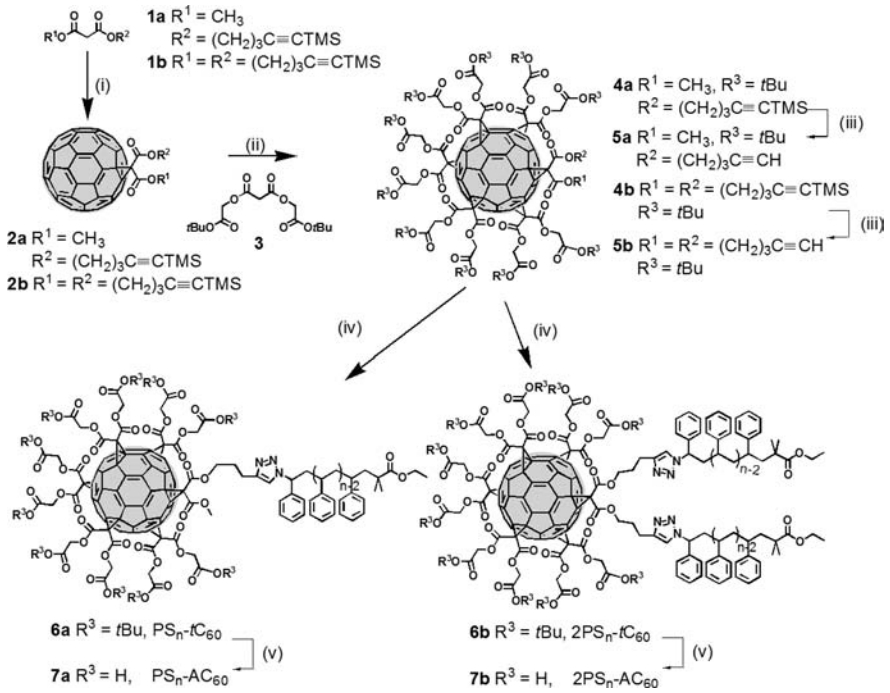

[a]Conditions: (i) C_{60}, toluene, I_2, DBU, rt (**2a**, 57%; **2b**, 51%); (ii) ODCB, I_2, DBU, rt (**4a**, 46%; **4b**, 45%); (iii) TBAF, THF (**5a**, 95%; **5b**, 80%); (iv) PS_n–N_3, toluene, CuBr, PMDETA, rt (**6a**, 80%; **6b**, 70%); (v) CH_2Cl_2, CF_3COOH, rt (**7a**, >95%; **7b**, >95%).

Information). The most convincing results confirming the chemical structure and purity of the final products were provided by electrospray ionization mass spectrometry (ESI–MS), which is a powerful technique for characterizing molecules with multiple ionizable groups. Ions with different charge states and shapes can be resolved by traveling wave ion mobility mass spectrometry (TWIM–MS) that enables gas-phase separation and complete deconvolution of the isotope patterns of ions with same m/z values.[59−61] Figure 1a shows the

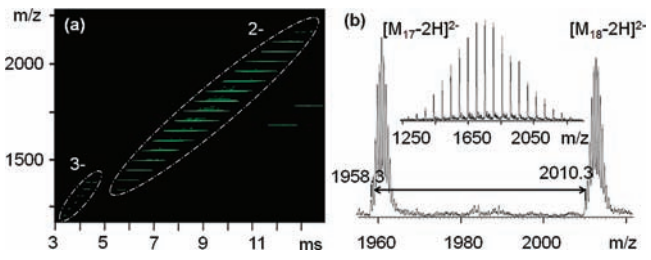

Figure 1. (a) 2D analysis of ESI–TWIM–MS spectrum of PS_{23}–AC_{60} with double and triple charged states circled. (b) 1D analysis of ESI–TWIM–MS spectrum of PS_{23}–AC_{60} for double charged state with zoom-in view of the spectrum to show the mass difference between two neighboring peaks and their monoisotopic patterns.

exemplary 2D ESI–TWIM–MS spectrum of PS_{23}–AC_{60} (drift time t vs m/z) where the doubly and triply charged species are shown as circled. The major distribution arises from charge state of 2−, which corresponds to $[PS_{23}–AC_{60}–2H]^{2-}$ with isotope spacing Δm = 0.5 amu. Figure 1b shows the actual 1D ESI–MS spectrum extracted from the 2− ions. A narrow molecular weight distribution can be observed with a spacing of 52.0 between neighboring peaks, which corresponds to the one repeating unit of PS with two charges (m/z = 104.1/2 = 52.0). The representative monoisotopic mass peak at m/z 2010.3 agrees well with the calculated value of 2010.2 for $[PS_{18}–AC_{60}–2H]^{2-}$. Although the distribution appears slightly lower than that obtained by ^{1}H NMR and SEC, it may be explained by the decreased ionizability and ESI efficiency in high molecular weight fractions. Table 1 summarizes the molecular characterizations of PS_n–AC_{60} and $2PS_n$–AC_{60} with various PS tail lengths, among which PS_{44}–AC_{60} and $2PS_{23}$–AC_{60} were purposely designed to possess identical overall molecular weight of PS, but with distinct molecular topology.

Micellization of Shape Amphphiles at Low Initial Molecular Concentrations [$C \leq 0.25$ (wt) %]. The solution self-assembly of these two series of shape amphiphiles was performed by adding selective solvent, water, to the solution in a common solvent, which was a mixture of 1,4-dioxane and DMF (w/w = 1/1). The critical water concentrations (C_{CWC}) in forming micelles was monitored by static light scattering (SLS) experiments. Figure 2 shows the SLS intensity changes with the water concentration for both series of PS_n–AC_{60} and $2PS_n$–AC_{60} at an initial molecular concentration of 0.1 (wt) %. The onset of scattering intensity increase appears at C_{CWC} where the self-assembled micelles start to form (see the positions pointed by the arrows where the slopes have a sudden increase in Figure 2a). For PS_n–AC_{60}, the observed value of C_{CWC} decreases from 19.0 (wt) % for PS_{23}–AC_{60} to 8.4 (wt) % for PS_{100}–AC_{60} (see also in Table 1). Note that the intensity change becomes sharper with increasing the PS tail length due to the formation of larger size of aggregates. Similarly in $2PS_n$–AC_{60} system, the observed C_{CWC} value decreases from 14.0 (wt) % of water for $2PS_{23}$–AC_{60} to 9.3 (wt) % for $2PS_{44}$–AC_{60} and the transitions also get sharper with increasing the PS tail length. Hence, the increased hydrophobicity of these shape amphiphiles was revealed by the decrease of in C_{CWC} as the PS tail length was increased.

dx.doi.org/10.1021/ja3000529 | J. Am. Chem. Soc. 2012, 134, 7780−7787

Table 1. Summary of Molecular Characterizations and Self-Assembly Parameters of PS_n–AC_{60} and $2PS_n$–AC_{60}

sample	N_{PS}[a]	M_n[b]	M_w/M_n[c]	topology[d]	morphology[e]	L (nm)[f]	C_{CWC} (%)[g]	S[h]
PS_{23}–AC_{60}	23	4.4k	1.06	I	S	5.5 ± 0.5	19.0	1.68
PS_{44}–AC_{60}	44	6.5k	1.01	I	S	6.4 ± 0.5	15.0	1.41
PS_{70}–AC_{60}	70	9.1k	1.02	I	S	6.9 ± 0.4	10.0	1.20
PS_{100}–AC_{60}	100	12.1k	1.01	I	S	8.0 ± 0.3	8.4	1.17
$2PS_{23}$–AC_{60}	23	6.8k	1.06	II	V	3.5 ± 0.3	14.0	1.07
$2PS_{30}$–AC_{60}	30	8.2k	1.04	II	V	4.0 ± 0.2	10.0	1.07
$2PS_{44}$–AC_{60}	44	11.0k	1.02	II	V	4.9 ± 0.2	9.3	1.08

[a]Degree of polymerization of the PS tail from SEC and ^{1}H NMR measurements. [b]Molecular weight calculated from M_n(PS) + M_n(AC_{60}). [c]Polydispersity index, measured by SEC, of corresponding PS_n–tC_{60} and $2PS_n$–tC_{60}. [d]Topology of shape amphiphiles (I, monotethered; II, ditethered). [e]Morphologies observed in TEM (S, sphere; V, vesicle) at an initial concentration of 0.1 wt %. [f]L is the hydrophobic PS chain dimension measured from TEM images. [g]C_{CWC} is the value of critical water content measured by SLS experiments at an initial concentration of 0.1 (wt) %. [h]S is the degree of stretching of PS tails.

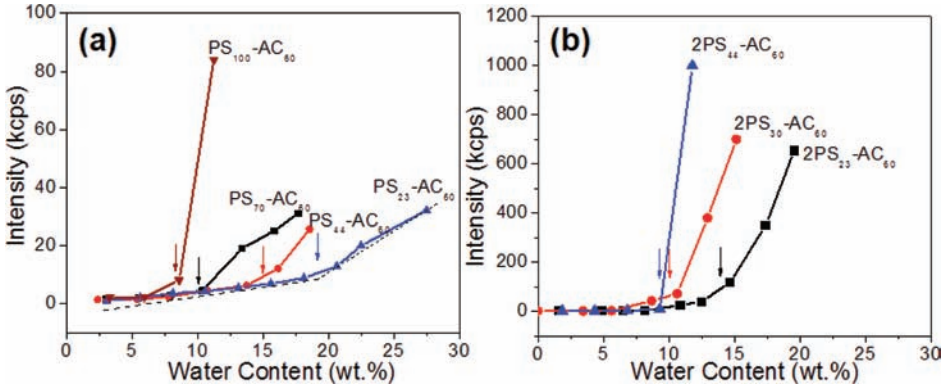

Figure 2. Light scattering intensity versus water content in the 1,4-dioxane/DMF/water system with an initial molecular concentration of 0.1 (wt) % for (a) PS_n–AC_{60} and (b) $2PS_n$–AC_{60}. The arrows show the critical water concentration (C_{CWC}) for the corresponding curves. The values of C_{CWC} are determined based on the point of intersection of the two tangent lines as shown by the dashed lines in panel a.

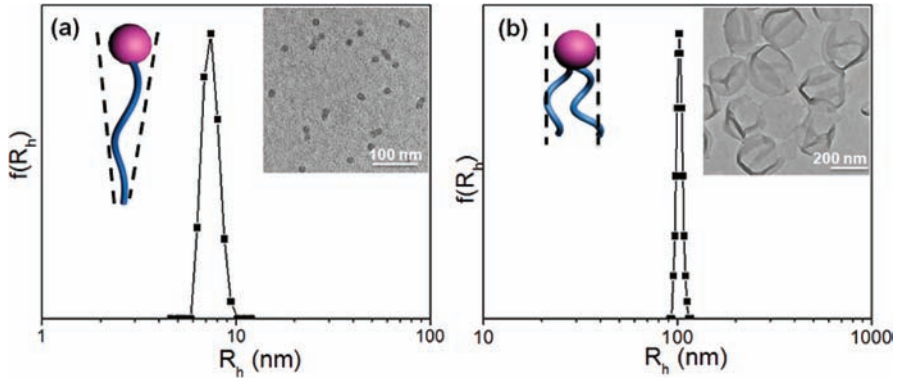

Figure 3. DLS results and TEM images (inset) of the self-assembled morphologies of (a) monotethered PS_{44}–AC_{60} and (b) ditethered $2PS_{23}$–AC_{60} in solution with a mixture of 1,4-dioxane and DMF (w/w = 1/1) as the common solvent and water as the selective solvent.

The self-assembled micellar morphologies were investigated by transmission electron microscopy (TEM) and dynamic light scattering (DLS) techniques. Figure 3 includes the TEM and DLS results of self-assemblies of PS_{44}–AC_{60} and $2PS_{23}$–AC_{60} at an initial molecular concentration of 0.1 (wt) %. Note that they are a pair of topological isomers. PS_{44}–AC_{60} forms spherical micelles with a hydrodynamic radius (R_h) centered at 7.0 nm, as revealed from CONTIN analysis of DLS results as shown in Figure 3a. $2PS_{23}$–AC_{60}, on the other hand, forms bilayered vesicles with $R_h \sim 100$ nm and a narrow size distribution measured from DLS in Figure 3b. The shape aspect ratio (P) of amphiphilic molecules was proposed by Israelachvili et al. to determine the self-assembled structures. It can be estimated by the ratio between cross-section areas of the head and tail ($\sigma_{head}/\sigma_{tail}$).[62] Since C_{60} has a well-defined structure and fixed volume, the smallest σ_{C60} of functionalized AC_{60} can be estimated to be 1.5 nm^2, assuming no salvation of the surface carboxylic acid groups.[63] In solution, the hydrodynamic size of AC_{60} is expected to be bigger as the degree of ionization of the surface carboxylic acid groups increases. The solvent properties also play a role. Similarly, the lower limit of σ_{PS} can be estimated to be 0.7 nm^2 assuming the PS tail is fully stretched.[64] Yet, since this value increases when the PS tail relaxes toward a random coil, it is highly dependent on the PS tail length.[65] Therefore, PS_{44}–AC_{60} with a stretched single tail is expected to be in a wedge-like molecular shape, while $2PS_{23}$–AC_{60} possesses a

dx.doi.org/10.1021/ja3000529 | J. Am. Chem. Soc. 2012, 134, 7780–7787

much smaller P due to topological requirements. Interestingly, in this low initial molecular concentration range, all of the PS_n–AC_{60} samples studied here form spherical micelles, while the series of $2PS_n$–AC_{60} forms bilayered vesicles disregarding the PS tail lengths (e.g., see Table 1). We speculate that this series of PS_n–AC_{60} holds the wedge-like molecular shape ($P > 1$) and the series of $2PS_n$–AC_{60} holds the cylindrical shape ($P \sim 1$) in this low molecular concentration range. It should be noted that the value of P could be changed as the self-assembly conditions vary, as shown in the high molecular concentration range of >0.25 (wt) % (vide infra).

The PS Tail Conformations: Stretched versus Relaxed. Hydrophobic PS tail conformations in micellar aggregates are important since they critically affect the formation and morphology of micelles, as well as their potential applications.[66] Hydrophobic alkyl chains in small-molecule surfactants are known to be highly stretched and even crystallized in certain cases.[67] Unlike small molecules, relatively flexible chain conformation is common for amphiphilic polymers, which results in a larger entropic contribution to the overall free energy during the micelle formation.[68] The subtle and delicate interplay between enthalpic and entropic contributions, thus, generates versatile morphologies for block copolymer micelles, associating with either stretching or compressing polymer chains to achieve free energy minimum.[48,69] The polymer tail conformation in the self-assembled aggregates of molecular shape amphiphiles has not yet been thoroughly explored. It is thus of interest to investigate the PS tail behaviors in the self-assemblies of these two series of shape amphiphiles and compare it to traditional surfactants and diblock copolymers. The stretching ratio of the PS tail in the micellar core can be characterized by

$$S = L/R_0 \quad (1)$$

where L is obtained from the core radius of micellar aggregates measured from TEM images subtracting the size of AC_{60} (Table 1). Note that half of the wall thickness should be utilized in the case of vesicles. R_0 is an average unperturbed (freely jointed) end-to-end distance of the PS tail length that can be calculated by[70]

$$R_0 = (N_{PS}/6.92)^{1/2} b \quad (2)$$

where N_{PS} is the degree of polymerization and b is the Kuhn length (b = 1.8 nm) for PS.

Figure 4 exhibits a plot of the stretching ratio, S, versus N_{PS} in spherical micelles of the series of PS_n–AC_{60} and the vesicles of the series of $2PS_n$–AC_{60}. It is evident that S decreases as the PS tail length increases in their spherical micelles of PS_n–AC_{60}, while it is almost independent of the PS tail length in the vesicles of this series of $2PS_n$–AC_{60}. Two quantitative linear relationships can be achieved in the double-logarithmic plot between S and N_{PS} (Figure S9 in Supporting Information), which suggests a scaling law of $S \sim N_{PS}^{-0.25}$ in the case of spherical micelles of the series of PS_n–AC_{60} and $S \sim N_{PS}^{0}$ in the vesicles of the $2PS_n$–AC_{60} series in the low initial molecular concentration range. Comparing the results of polystyrene-*block*-poly(acrylic acid) (PS-*b*-PAA) block copolymer micelles where $S \sim N_{PS}^{-0.1} N_{PAA}^{-0.15}$, the stretching ratio of the PS tails exhibits a stronger dependency in PS_n–AC_{60} spheres but is almost independent of the PS tail length in $2PS_n$–AC_{60} vesicles. The decreasing stretching ratio with increasing PS tail length in the series of PS_n–AC_{60} molecular shape amphiphiles indicates that micellar behaviors of the PS_n–AC_{60} are small molecular surfactant-like with shorter PS tail lengths and become more amphiphilic block copolymer-like when the PS tail length gets longer.

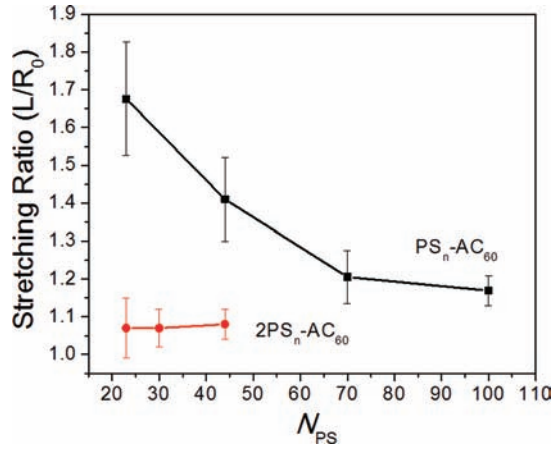

Figure 4. Plotting of stretching ratio S versus the PS chain length N_{PS} for PS_n–AC_{60} and $2PS_n$–AC_{60}.

Micellization of Shape Amphphiles at Relatively High Initial Molecular Concentrations [C > 0.25 (wt) %] and the Morphological Phase Diagram of the Series of PS_n–AC_{60}. The series of PS_n–AC_{60} forms versatile self-assembled morphologies at higher initial molecular concentrations [C > 0.25 (wt) %]. In contrast, only a single vesicular morphology is observed for $2PS_n$–AC_{60} system under the identical conditions. Figure 5 is a set of TEM bright images of self-assembled micelles of PS_{70}–AC_{60} at different initial molecular concentrations. It is evident that the morphology changes from spherical micelles with an initial concentration of 0.1 (wt) %, to worm-like cylinders network at 0.5 (wt) %, to a mixed morphology of cylinders and vesicles at 1.0 (wt) %, and finally to pure vesicles when the initial concentration reaches 2.0 (wt) %. The morphological transitions of all of PS_n–AC_{60} molecular shape amphiphiles at initial molecular concentrations ranging from 0.1 to 2 (wt) % are summarized in Figure 6. To the best of our knowledge, this is the first experimentally acquired phase diagram for shape amphiphiles. As discussed previously, all of this series of PS_n–AC_{60} form spherical micelles at a low initial molecular concentration range between 0.1 and 0.25 (wt) %. Transitions from spheres to cylinders and further to vesicles take place at higher initial molecular concentrations [C > 0.25 (wt) %], and these transitions appear at lower initial molecular concentrations for those PS_n–AC_{60} with longer PS tails.

To explain the results in Figure 6, we need to consider the driving force of these micellar morphological transitions. First, the aggregation number of micelles (N_{agg}) increases with increasing the molecular concentration (C), which follows the relationship $N_{agg} = (C/C_{CMC})^{1/2}$, where C_{CMC} is the critical micelle concentration.[62] Second, the concentration of free counterions (H^+) has strong affects on the self-assembly behaviors of charged micelles.[71,72] The concentration of free counterions always increases with increasing the initial molecular concentration.[73] This could be validated by measuring the pH value of the micellar solutions at different initial molecular concentrations. For instance, the measured pH value of PS_{70}–AC_{60} decreases from ca. 5.5 at an initial molecular concentration of 0.1 (wt) % to ca. 4.3 at an initial molecular concentration of 2.0 (wt) %, indicating an increase of the concentration of free counterions (H^+). At the same time,

dx.doi.org/10.1021/ja3000529 | J. Am. Chem. Soc. 2012, 134, 7780–7787

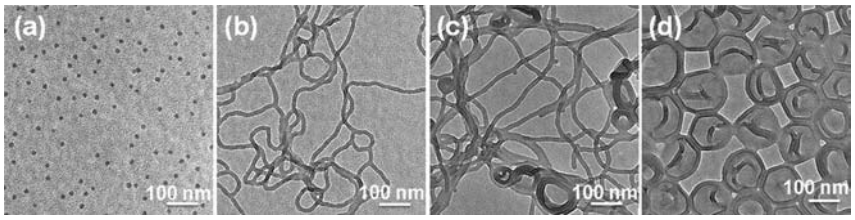

Figure 5. TEM images of self-assembly morphologies of PS_{70}–AC_{60} with different initial molecular concentrations in the 1,4-dioxane/DMF/water system: (a) 0.1; (b) 0.5; (c) 1.0; (d) 2.0 (wt) %.

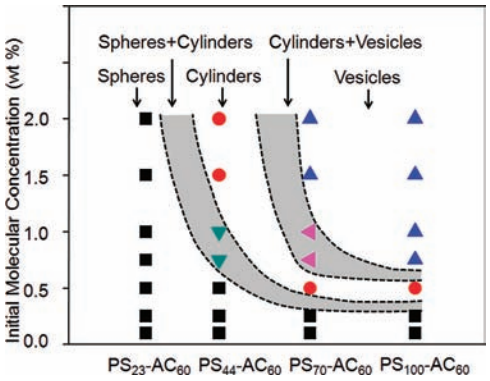

Figure 6. Morphological phase diagram of PS_n–AC_{60} self-assemblies in the 1,4-dioxane/DMF/water system depending on the initial molecular concentration and the PS tail length.

the degree of ionization (α) of the carboxylic acid groups decreases with increasing the initial molecular concentration, which follows the relationship $\alpha \propto (k_a/C)^{1/2}$ where k_a is the averaged dissociation constant of each carboxylic acid.[74] To minimize the free energy of micelles, the equilibrium micellar morphologies will favor larger aggregates with lower charge density. Therefore, spherical micelles are pushed to transfer to cylinders and further to vesicles with increasing the initial molecular concentration.

Furthermore, these transitions are also closely associated with the relaxation of the stretched PS tails in the micellar cores. Since the PS_n–AC_{60} with a longer PS tail lengths possess less stretching and thus, they also favor the morphological transitions (the entropic contribution). This is exactly the experimental observation in the case of PS_{100}–AC_{60}. These micellar morphology transitions can also be simply understood by the value of shape aspect ratio, *P*. According to the Gouy–Chapman theory,[66] the hydrodynamic size of AC_{60} will decrease as increasing the initial molecular concentration and the concentration of free counterions, which results in a decrease of *P*. This explains the dependence of morphological transition on the initial molecular concentration (see Figure 6 for PS_{70}–AC_{60}). Meanwhile, as discussed in the previous section, the PS tails become less stretched as their tails length increase, which leads to an increase of the σ_{PS} and, thus, a decrease of *P*. Indeed, the micellar morphologies did change from spheres to cylinders and further to vesicles as increasing the PS tail length at a fixed molecular concentration [e.g., see Figure 6 at 2.0 (wt) %]. Overall, the value of *P* decreases from the lower left to the upper right quadrant of Figure 6, driving these micellar morphological transitions as observed. Hence, the versatile morphologies in the narrow range of initial concentration for this series of shape amphiphile could be attributed to the delicate balance between σ_{C60} and σ_{PS}. Compared with the initial molecular concentration effects on small molecular surfactants and amphiphilic block copolymers, this sharp dependence of micellar morphology on the initial concentrations of PS_n–AC_{60} is rather unusual.[75,76] For instance, the micellar morphology of polystyrene$_{310}$-*b*-poly(acrylic acid)$_{52}$ changes from cylinders to a mixture of cylinders and vesicles when its initial concentration changes from 0.1 to 10 (wt) %.[49]

CONCLUSION

In summary, two series of precisely defined molecular shape amphiphiles with distinct topology (PS_n–AC_{60} and $2PS_n$–AC_{60}) have been designed and synthesized via regiospecific functionalization of C_{60} and subsequent "click" reaction with hydrophobic PS chains. Micellar morphologies were observed from their self-assembly with a mixture of 1,4-dioxane and DMF (w/w = 1/1) as the common solvent and water as the selective solvent, and have been systematically studied with respect to the molecular parameters such as molecular topology and PS tail length, and the solution parameters such as initial molecular concentration. First, the effect of molecular topology on micellar morphology has been studied at a low initial molecule concentration of equal or less than 0.25 (wt) %. All of this series of PS_n–AC_{60} forms the spherical micelles, while the series of $2PS_n$–AC_{60} forms the bilayered vesicles. The stretching ratio, *S*, of the PS tails in the spherical micelles exhibits a stronger dependency in this series of PS_n–AC_{60}, yet in the series of $2PS_n$–AC_{60} vesicles, this ratio is almost independent of the PS tail length. Even in spheres of the series of PS_n–AC_{60}, the stretching ratio of PS tails decreases as increasing the PS tail length, indicating that the micelle behavior in the shorter PS tails is more close to that of small-molecule surfactant-like, while as the PS tail length increases, the micelle behavior is gradually shifted to that of amphiphilic block copolymer-like. Second, when the initial molecular concentration is increased to above 0.25 (wt) %, the series of PS_n–AC_{60} exhibits micellar morphological transitions from spheres to cylinders and further to vesicles with increasing the initial molecular concentration and/or the PS tail length. However, only bilayered vesicles can be observed for the series of $2PS_n$–AC_{60} even in this relatively high molecular concentration range. On the basis of the experimental results, a morphological phase diagram for the series of PS_n–AC_{60} was constructed with respect to both the PS tail length and the initial molecular concentration. The driving force of these transitions is attributed to increasing both the size of self-assembled aggregates and the concentration of free counterions. Such morphological transitions are also closely associated with the decreasing value of shape aspect ratio, *P*. The versatile self-assembled morphologies exhibited in such a narrow initial molecular concentration are attributed to the delicate balance between cross-section area of the σ_{C60} and σ_{PS}. The present work provides the first comprehensive study of phase behaviors of molecular shape amphiphiles in solution. The versatile and

dx.doi.org/10.1021/ja3000529 | J. Am. Chem. Soc. 2012, 134, 7780–7787

concentration-sensitive phase behaviors of these molecular shape amphiphiles are unique. These giant molecular shape amphiphiles, thus, represent a novel class of amphiphilic molecules that have not been systematically explored beyond the traditional surfactants and block copolymers systems, which provides a new platform for understanding supramolecular self-assemblies of shape amphiphilic molecules in solution.

■ ASSOCIATED CONTENT

Supporting Information

Additional information on the synthesis and characterization of the compounds. This material is available free of charge via the Internet at http://pubs.acs.org.

■ AUTHOR INFORMATION

Corresponding Author

scheng@uakron.edu

Notes

The authors declare no competing financial interest.

■ ACKNOWLEDGMENTS

This research was supported by the National Science Foundation (DMR-0906898, DMR-0821313, and CHE-1012636). The generous research funding supported by The Joint-Hope Education Foundation is gratefully acknowledged.

■ REFERENCES

(1) Whitesides, G. M.; Mathias, J.; Seto, C. *Science* **1991**, *254*, 1312–1319.
(2) Whitesides, G. M.; Boncheva, M. *Proc. Nat. Acad. Sci. U.S.A.* **2002**, *99*, 4769–4774.
(3) Philp, D.; Stoddart, J. F. *Angew. Chem., Int. Ed.* **1996**, *35*, 1154–1196.
(4) Zhao, D.; Huo, Q.; Feng, J.; Chmelka, B. F.; Stucky, G. D. *J. Am. Chem. Soc.* **1998**, *120*, 6024–6036.
(5) Antonietti, M.; Förster, S. *Adv. Mater.* **2003**, *15*, 1323–1333.
(6) Leininger, S.; Olenyuk, B.; Stang, P. J. *Chem. Rev.* **2000**, *100*, 853–908.
(7) Simard, M.; Su, D.; Wuest, J. D. *J. Am. Chem. Soc.* **1991**, *113*, 4696–4698.
(8) Winfree, E.; Liu, F.; Wenzler, L. A.; Seeman, N. C. *Nature* **1998**, *394*, 539–544.
(9) Leibler, L. *Macromolecules* **1980**, *13*, 1602–1617.
(10) Malmsten, M.; Lindman, B. *Macromolecules* **1992**, *25*, 5440–5445.
(11) Zhang, L.; Eisenberg, A. *Science* **1995**, *268*, 1728–1731.
(12) Rolland, J. P.; Maynor, B. W.; Euliss, L. E.; Exner, A. E.; Denison, G. M.; DeSimone, J. M. *J. Am. Chem. Soc.* **2005**, *127*, 10096–10100.
(13) Zhang, Z.; Horsch, M. A.; Lamm, M. H.; Glotzer, S. C. *Nano Lett.* **2003**, *3*, 1341–1346.
(14) Percec, V.; Ahn, C. H.; Ungar, G.; Yeardley, D. J. P.; Moller, M.; Sheiko, S. S. *Nature* **1998**, *391*, 161–164.
(15) Percec, V.; Wilson, D. A.; Leowanawat, P.; Wilson, C. J.; Hughes, A. D.; Kaucher, M. S.; Hammer, D. A.; Levine, D. H.; Kim, A. J.; Bates, F. S.; Davis, K. P.; Lodge, T. P.; Klein, M. L.; DeVane, R. H.; Aqad, E.; Rosen, B. M.; Argintaru, A. O.; Sienkowska, M. J.; Rissanen, K.; Nummelin, S.; Ropponen, J. *Science* **2010**, *328*, 1009–1014.
(16) Chen, Q.; Bae, S. C.; Granick, S. *Nature* **2011**, *469*, 381–384.
(17) Glotzer, S. C.; Solomon, M. J. *Nat. Mater.* **2007**, *6*, 557–562.
(18) Horsch, M. A.; Zhang, Z.; Glotzer, S. C. *Phys. Rev. Lett.* **2005**, *95*, 056105.
(19) Glotzer, S. C.; Horsch, M. A.; Iacovella, C. R.; Zhang, Z.; Chan, E. R.; Zhang, X. *Curr. Opin. Colloid Interface Sci.* **2005**, *10*, 287–295.
(20) Iacovella, C. R.; Keys, A. S.; Horsch, M. A.; Glotzer, S. C. *Phys. Rev. E* **2007**, *75*, 040801.
(21) Zhang, X. *J. Chem. Phys.* **2005**, *123*, 184718.
(22) Parak, W. J.; Pellegrino, T.; Micheel, C. M.; Gerion, D.; Williams, S. C.; Alivisatos, A. P. *Nano Lett.* **2002**, *3*, 33–36.
(23) DeVries, G. A.; Brunnbauer, M.; Hu, Y.; Jackson, A. M.; Long, B.; Neltner, B. T.; Uzun, O.; Wunsch, B. H.; Stellacci, F. *Science* **2007**, *315*, 358–361.
(24) Mirkin, C. A.; Letsinger, R. L.; Mucic, R. C.; Storhoff, J. J. *Nature* **1996**, *382*, 607–609.
(25) Westenhoff, S.; Kotov, N. A. *J. Am. Chem. Soc.* **2002**, *124*, 2448–2449.
(26) Petukhova, A.; Greener, J.; Liu, K.; Nykypanchuk, D.; Nicolaÿ, R.; Matyjaszewski, K.; Kumacheva, E. *Small* **2012**, *8*, 731–737.
(27) Velonia, K.; Rowan, A. E.; Nolte, R. J. M. *J. Am. Chem. Soc.* **2002**, *124*, 4224–4225.
(28) Boerakker, M. J.; Hannink, J. M.; Bomans, P. H. H.; Frederik, P. M.; Nolte, R. J. M.; Meijer, E. M.; Sommerdijk, N. A. J. M. *Angew. Chem., Int. Ed.* **2002**, *41*, 4239–4241.
(29) Boerakker, M. J.; Botterhuis, N. E.; Bomans, P. H. H.; Frederik, P. M.; Meijer, E. M.; Nolte, R. J. M.; Sommerdijk, N. A. J. M. *Chem.—Eur. J.* **2006**, *12*, 6071–6080.
(30) Reynhout, I. C.; Cornelissen, J. J. L. M.; Nolte, R. J. M. *J. Am. Chem. Soc.* **2007**, *129*, 2327–2332.
(31) Weis, C.; Friedrich, C.; Muelhaupt, R.; Frey, H. *Macromolecules* **1995**, *28*, 403–405.
(32) Zhang, W.-B.; Tu, Y.; Ranjan, R.; Van Horn, R. M.; Leng, S.; Wang, J.; Polce, M. J.; Wesdemiotis, C.; Quirk, R. P.; Newkome, G. R.; Cheng, S. Z. D. *Macromolecules* **2008**, *41*, 515–517.
(33) Zhou, P.; Chen, G.-Q.; Li, C.-Z.; Du, F.-S.; Li, Z.-C.; Li, F.-M. *Chem. Commun.* **2000**, 797–798.
(34) Kawauchi, T.; Kumaki, J.; Yashima, E. *J. Am. Chem. Soc.* **2005**, *127*, 9950–9951.
(35) Cardoen, G.; Coughlin, E. B. *Macromolecules* **2004**, *37*, 5123–5126.
(36) Zhang, W.; Fang, B.; Walther, A.; Müller, A. H. E. *Macromolecules* **2009**, *42*, 2563–2569.
(37) Knischka, R.; Dietsche, F.; Hanselmann, R.; Frey, H.; Mülhaupt, R.; Lutz, P. J. *Langmuir* **1999**, *15*, 4752–4756.
(38) Lee, W.; Ni, S.; Deng, J.; Kim, B.-S.; Satija, S. K.; Mather, P. T.; Esker, A. R. *Macromolecules* **2007**, *40*, 682–688.
(39) Hirsch, A.; Brettreich, M. *Fullerenes: Chemistry and Reactions*; Wiley-VCH: Weinheim, 2005.
(40) Zhou, S.; Burger, C.; Chu, B.; Sawamura, M.; Nagahama, N.; Toganoh, M.; Hackler, U. E.; Isobe, H.; Nakamura, E. *Science* **2001**, *291*, 1944–1947.
(41) Schade, B.; Ludwig, K.; Böttcher, C.; Hartnagel, U.; Hirsch, A. *Angew. Chem., Int. Ed.* **2007**, *46*, 4393–4396.
(42) Homma, T.; Harano, K.; Isobe, H.; Nakamura, E. *J. Am. Chem. Soc.* **2011**, *133*, 6364–6370.
(43) Muñoz, A.; Illescas, B. M.; Sánchez-Navarro, M.; Rojo, J.; Martín, N. *J. Am. Chem. Soc.* **2011**, *133*, 16758–16761.
(44) Yu, H.; Gan, L. H.; Hu, X.; Gan, Y. Y. *Polymer* **2007**, *48*, 2312–2321.
(45) Yu, X.; Zhong, S.; Li, X.; Tu, Y.; Yang, S.; Van Horn, R. M.; Ni, C.; Pochan, D. J.; Quirk, R. P.; Wesdemiotis, C.; Zhang, W.-B.; Cheng, S. Z. D. *J. Am. Chem. Soc.* **2010**, *132*, 16741–16744.
(46) Zhang, W.-B.; Li, Y.; Li, X.; Dong, X.; Yu, X.; Wang, C.-L.; Wesdemiotis, C.; Quirk, R. P.; Cheng, S. Z. D. *Macromolecules* **2011**, 2589–2596.
(47) Hayward, R. C.; Pochan, D. J. *Macromolecules* **2010**, *43*, 3577–3584.
(48) Zhang, L.; Eisenberg, A. *J. Am. Chem. Soc.* **1996**, *118*, 3168–3181.
(49) Shen, H.; Eisenberg, A. *J. Phys. Chem. B* **1999**, *103*, 9473–9487.
(50) Liu, F.; Eisenberg, A. *J. Am. Chem. Soc.* **2003**, *125*, 15059–15064.
(51) Yang, S.; Yu, X.; Wang, L.; Tu, Y.; Zheng, J. X.; Xu, J.; Van Horn, R. M.; Cheng, S. Z. D. *Macromolecules* **2010**, *43*, 3018–3026.
(52) Zhang, S.; Lukoyanova, O.; Echegoyen, L. *Chem.—Eur. J.* **2006**, *12*, 2846–2853.

(53) Hirsch, A.; Lamparth, I.; Karfunkel, H. R. *Angew. Chem., Int. Ed.* **1994**, *33*, 437−438.
(54) Bingel, C. *Chem. Ber.* **1993**, *126*, 1957−1959.
(55) Iehl, J.; Nierengarten, J.-F. *Chem. Commun.* **2010**, *46*, 4160−4162.
(56) Kolb, H. C.; Finn, M. G.; Sharpless, K. B. *Angew. Chem., Int. Ed.* **2001**, *40*, 2004−2021.
(57) Dong, X.-H.; Zhang, W.-B.; Li, Y.; Huang, M.; Zhang, S.; Quirk, R. P.; Cheng, S. Z. D. *Polymer Chem.* **2012**, *3*, 124−134.
(58) Iehl, J.; Pereira de Freitas, R.; Delavaux-Nicot, B.; Nierengarten, J.-F. *Chem. Commun.* **2008**, 2450−2452.
(59) Chan, Y.-T.; Li, X.; Soler, M.; Wang, J.-L.; Wesdemiotis, C.; Newkome, G. R. *J. Am. Chem. Soc.* **2009**, *131*, 16395−16397.
(60) Perera, S.; Li, X.; Soler, M.; Schultz, A.; Wesdemiotis, C.; Moorefield, C. N.; Newkome, G. R. *Angew. Chem., Int. Ed.* **2010**, *49*, 6539−6544.
(61) Song, J.; Grün, C. H.; Heeren, R. M. A.; Janssen, H.-G.; van den Brink, O. F. *Angew. Chem., Int. Ed.* **2010**, *49*, 10168−10171.
(62) Israelachvili, J. N.; Mitchell, D. J.; Ninham, B. W. *J. Chem. Soc., Faraday Trans. 2* **1976**, *72*, 1525−1568.
(63) Lamparth, I.; Maichle-Mössmer, C.; Hirsch, A. *Angew. Chem., Int. Ed.* **1995**, *34*, 1607−1609.
(64) Privalko, V. P. *Macromolecules* **1980**, *13*, 370−372.
(65) Kumaki, J. *Macromolecules* **1988**, *21*, 749−755.
(66) Evans, F.; Wennerstrom, H. *The Colloidal Domain: Where Physics, Chemistry, Biology, And Technology Meet*, 2nd ed.; Wiley-VCH: New York, 1999.
(67) Holmberg, K.; JÖnsson, B.; Kronberg, B.; Lindman, B. *Surfactants and Polymers in Aqueous Solution*, 2nd ed.; John Wiley & Sons Ltd: England, 2003.
(68) Bhargava, P.; Zheng, J. X.; Li, P.; Quirk, R. P.; Harris, F. W.; Cheng, S. Z. D. *Macromolecules* **2006**, *39*, 4880−4888.
(69) Bhargava, P.; Tu, Y.; Zheng, J. X.; Xiong, H.; Quirk, R. P.; Cheng, S. Z. D. *J. Am. Chem. Soc.* **2007**, *129*, 1113−1121.
(70) Rubinstein, M.; Colby, R. H. *Polymer Physics*, 1st ed.; Oxford University Press: Oxford, 2003.
(71) Quirion, F.; Magid, L. J. *J. Phys. Chem.* **1986**, *90*, 5435−5441.
(72) Bernheim-Groswasser, A.; Zana, R.; Talmon, Y. *J. Phys. Chem. B* **2000**, *104*, 4005−4009.
(73) Mysels, K. J. *J. Colloid Sci.* **1955**, *10*, 507−522.
(74) Miessler, G. *Inorganic Chemistry*. Prentice Hall: Englewood Cliffs, NJ , 1991.
(75) Zhang, L.; Eisenberg, A. *Macromolecules* **1999**, *32*, 2239−2249.
(76) Alargova, R. G.; Danov, K. D.; Petkov, J. T.; Kralchevsky, P. A.; Broze, G.; Mehreteab, A. *Langmuir* **1997**, *13*, 5544−5551.